Toward a New Generation of Electrically Controllable Hygromorphic Soft Actuators

Silvia Taccola, Francesco Greco,* Edoardo Sinibaldi, Alessio Mondini, Barbara Mazzolai, and Virgilio Mattoli**

The emergence of responsive polymers is of fundamental interest, and their ability to reversibly reply to a given stimulus, such as heat, electric voltage, or light, has practical applications in several fields, including soft robotics, active sensing, and actuation.[1] Notably, conjugated polymers (CP), such as polypyrrole (PPy), polyaniline, and poly(3,4-ethylenedioxythiophene) (PEDOT), have shown great potential with respect to actuation and significant efforts have been focused in particular on the realization of "dry" CP actuators that can function in air.[2] Recently, Okuzaki et al.[3] proposed a new class of CP actuators that function in ambient air based on the cooperation between the electrical conductivity and hygroscopic nature of conductive polymers. These authors discovered that electrochemically synthesized PPy films exhibit a significant reversible volume expansion in air resulting from the absorption and desorption of water vapor present in ambient air.[4] Furthermore, a volume contraction was observed under the application of an electric current, which was attributed to the desorption of water vapor as a result of Joule heating.[5] A similar electrically induced isotropic dimensional change was subsequently observed in ≈20 µm thick poly(3,4-ethylenedioxythiophene):polystyrene sulfonate (PEDOT:PSS) films prepared using the solution-casting method.[6] The ubiquitous presence of humidity in ambient air and its variation makes the development of humidity-responsive actuators both appealing and of importance. By chance, the capability to convert simple environmental stimuli, such as humidity, into mechanical reversible motion is regularly observed in living systems, particularly plants.[7] These systems are capable of converting the sorption and desorption of water into driving forces for movement. A well-known example is the release of ripe seeds from pine cones, which open due to a bending movement of their scales during drying in ambient air and close in wet conditions.[8] Similarly, seeds from wild wheat are propelled into soil after being released, which is solely due to the daily change in humidity that induces a curvature of the awns depending on the moisture level.[9] Interestingly, many actuation systems in plants have a common structural feature: the humidity-responsive actuation results from the coupling of two differently structured tissue layers with different elongations along a specific direction. These layers are interfacially bound to each other to form a laminated, double-layered composite structure.[10] Although the aforementioned actuators developed by Okuzaki's group undergo isotropic dimensional changes, anisotropic motions have not been thoroughly explored. Inspired by the differential swelling or shrinking of natural double-layered structures, one approach for achieving anisotropic motion in artificial actuators is to use a bilayer system in which the active layer is composed of a humidity-responsive material and the other layer is a passive material that is inert to humidity, that provides mechanical strength and that converts the isotropic volume change into a bending motion. In this work, we present a double-layered, anisotropic humidity-driven actuator based on an ultrathin active layer of PEDOT:PSS and a passive layer composed of poly(dimethylsiloxane) (PDMS), with intrinsic sensing capability, and able to be controlled both by joule effect or directly by environmental humidity variations.

PDMS elastomer was selected as the passive substrate because of its elasticity, good flexibility, chemical and humidity inertness, remarkable durability against repeated deformation, and resistance to high temperature. Because of these properties, in our system, PDMS should easily deform as a result of the contraction/expansion of the active layer and should withstand repeated and reversible deformation. PEDOT:PSS was selected as the active material due to the good combination of several features that influence actuator performance, such as its suitable electrical conductivity, humidity responsiveness, mechanical properties, and chemical and thermal stability.[11] Moreover, PEDOT:PSS is commercially available in the form of a ready-to-use waterborne dispersion; therefore, the active conducting polymer layer can be deposited by spin-coating, which results in a well-controlled homogeneous and reproducible thickness in a range between a few tens to several hundreds of nanometers, as we reported in some recent works.[12]

The proposed actuator has the potential to simultaneously combine active/passive actuation and sensing within a single-composite material. Movement can be controlled through the application of an electric current or by changes in environmental humidity (**Figure 1**a and Video S1, Supporting Information). In addition to actuation, the hygroscopic properties of the PEDOT:PSS layer impart sensing capabilities because a variation in the environmental humidity induces a reversible, reproducible variation in its electrical resistance, typically on the order of 1.25%/10% relative humidity (RH).[12c] Furthermore, because of the piezoresistive behavior of PEDOT:PSS, where its gauge factor has been reported to be between 5.2 and 17.8, this material has been proposed for use as a sensitive layer in strain and touch sensors.[13]

Dr. S. Taccola, Dr. F. Greco, Dr. E. Sinibaldi, Dr. A. Mondini, Dr. B. Mazzolai, Dr. V. Mattoli
Center for Micro-BioRobotics @SSSA
Istituto Italiano di Tecnologia
Viale Rinaldo Piaggio 34, Pontedera 56025, Italy
E-mail: silvia.taccola@iit.it; francesco.greco@iit.it; virgilio.mattoli@iit.it

DOI: 10.1002/adma.201404772

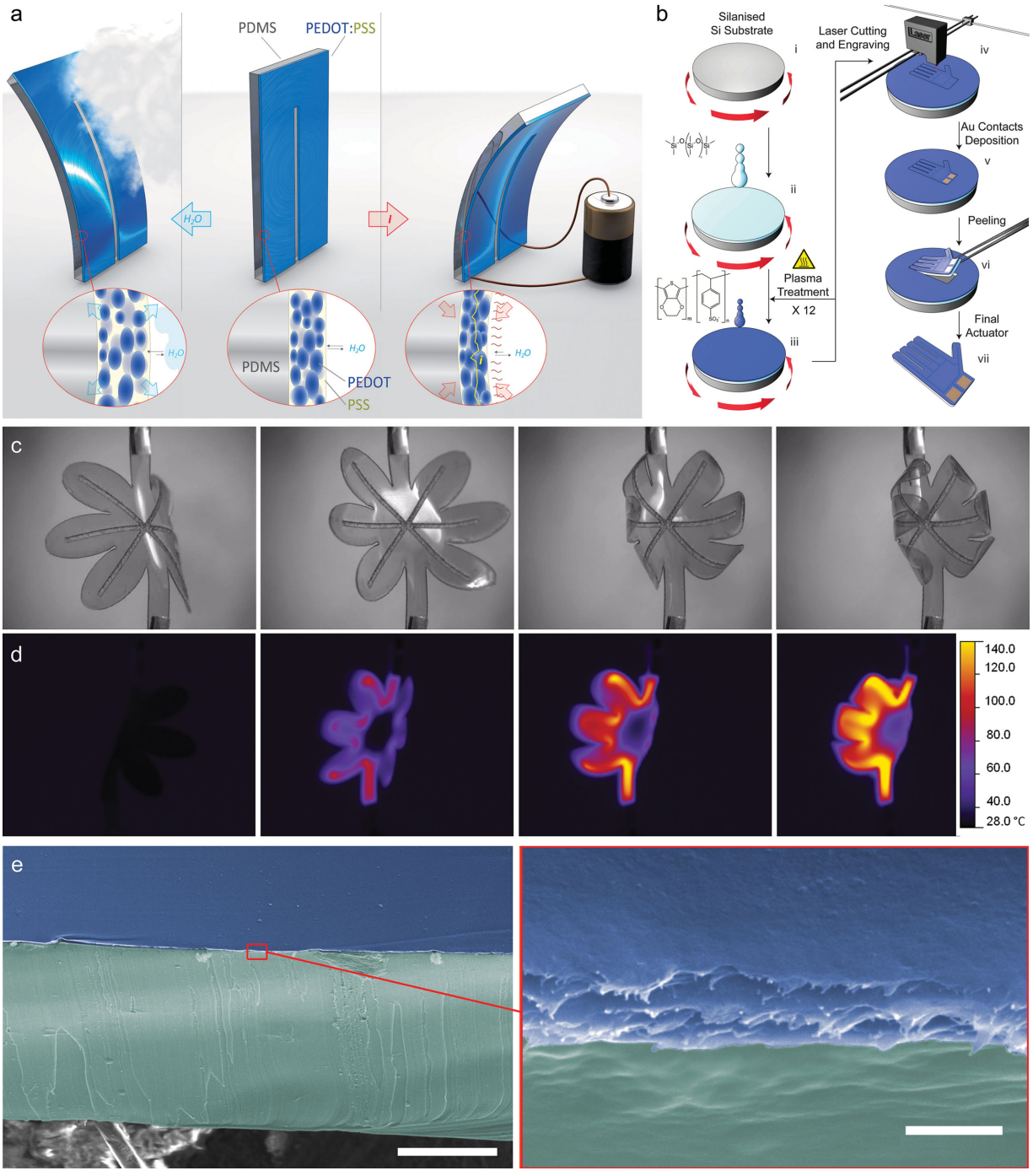

Figure 1. a) Schematic representation of the working principle behind the actuators based on the sorption/desorption of environmental moisture: beginning from the original position (central), in which the actuator is in equilibrium with its environment, the application of an electric current drives a contraction of the PEDOT:PSS layer due to Joule-heating-induced water desorption, which subsequently induces a bending motion toward the PEDOT:PSS layer (right); in the reverse process, as the environmental moisture content increases, the actuator bends from its original position toward the PDMS layer due to the sorption of water until a new equilibrium is established (left). b) Overview of the actuator fabrication process: (i) silanization of the silicon wafer; (ii) deposition of the PDMS layer by spin coating; (iii) air plasma treatment and deposition of PEDOT:PSS (12 layers) by spin coating; (iv) laser cutting and patterning; (v) deposition of gold electrodes by DC sputtering; and (vi) peeling of the bilayer. c) Actuation movement of an electrically driven flower-shaped actuator and corresponding thermal images. d) When a voltage is applied between the electrodes, the pattern drives the flow of current along each petal, which allows the structure to fold (see also Video S3, Supporting Information). e) Scanning electron microscopy (SEM) images (40° tilted view) of a cross section of the PEDOT:PSS/PDMS bilayer, which was cut using a razor blade. The magnification of the left image is 800× (scale bar represents 50 μm), and the magnification of the right image is 80 000× (scale bar represents 500 nm). The image was postcolorized: the PDMS layer is green, and the PEDOT:PSS layer is blue.

All of the aforementioned unique features along with the tailorability of the fabrication process provide possibilities for a series of interesting applications for these structures as active bioinspired elements with intrinsic sensing and actuation capabilities.

A schematic representation of the developed fabrication procedure (see also Experimental Section), is shown in Figure 1b. We followed a mask-free, time- and material-saving approach based on direct machining of the PEDOT:PSS/PDMS structures using a commercial CO_2 laser cutting system, which allowed actuators to be fabricated with different shapes and circuit patterns (see Video S2, Supporting Information). By varying the laser cutting parameters, we were able to simultaneously cut and pattern the surface of the actuators, thereby avoiding misalignment problems and reducing the processing time and manipulation. The patterning of the active surface in the form of electric circuits was performed by engraving only a thin PEDOT:PSS layer. This allowed the current flow between the electrodes to be driven along specific paths, thereby inducing local bending of selected portions of the structure (Figure 1c–d). Due to the silanization of the silicon wafers, the PEDOT:PSS/PDMS structures could easily be peeled off from the substrate after laser machining and used as free-standing actuators. The electrical connection was easily established using small flat alligator clips.

Notably, the ratio of the active-to-passive layer thickness is extremely small, as clearly evidenced in the scanning electron microscopy (SEM) images of an actuator cross section (Figure 1e), in which the thicknesses of the PEDOT:PSS and PDMS layers were 600 ± 29 nm and 120 ± 10 µm, respectively. The maximum moisture desorption-related contraction in PEDOT:PSS was estimated to be on the order of 2%.[6] Despite the thinness of the active layer, the properties of the selected materials and the actuator design are such that this small contraction is capable of causing a large bending displacement of the relatively thick bilayer. However, the use of a thin active layer allows for a rapid sorption/desorption of water, which results in a rapid actuation time. Moreover, the PEDOT:PSS film is characterized by a multilayered structure due to the multiple spin-coating deposition steps (magnified part of Figure 1e). We believe that this stacked layer microstructure has a beneficial role in relaxing the stress induced by bending and in reducing the effect of crack propagation within the active layer.

For characterization, the electro-thermo-mechanical responses of our actuators were tested on beam-shaped structures. To evaluate how the surface patterns affect actuator performance, three beam structures were fabricated (namely s1, s2, s3) that had the same dimensions (3 mm wide, 10 mm long) but different pattern lengths (h = 2, 5, and 8 mm, respectively) above the base of the beam (**Figure 2**a). The resistances of the resulting conductive paths were 1.13 ± 0.03, 1.63 ± 0.03, and 2.50 ± 0.18 kΩ for samples s1, s2, and s3, respectively. The electro-thermomechanical characterization was performed on cantilever beams in which one end was fixed and the other end was free to move. A rectangular area was provided at one end of the beam for clamping and for the electrical connection. Step input voltages of 5, 10, 15, 20, 25, and 30 V were applied to the samples, and the resulting bending displacements were recorded using a digital camera. Depending on the pattern length, different portions of the beam were heated by the current, which induced different bending behaviors (Figure 2a). Indeed, s3 was bent along almost its entire length, i.e., almost to the tip, whereas s1 and s2 exhibited shorter bending regions, which corresponded to the heated portion, with the rest of beam remaining essentially straight. For each input voltage, the surface temperature, curvature, and blocking force were determined, and the measurement results are summarized in Figure 2b–d. Regarding the surface temperature, the actuators were tested up to a maximum temperature of ≈200 °C, which was considered to be the safe limit for reliable performance of the materials. The three samples exhibited a linear temperature increase as the power increased and an increased curve slope as the pattern length decreased (Figure 2b). This trend was expected because a longer line pattern (s3) resulted in heating throughout a wider portion of the actuator compared with that of a smaller portion (s1, s2); hence, a lower temperature was reached under the same applied power. The curvatures of samples s1–3 were estimated by image processing, as described in the Experimental Section, by considering the heated beam portions. Examples of the processed images are presented in Figure S1 (Supporting Information), in which a straight portion closer to the tip is clearly visible, particularly for higher curvatures. As expected, at the same temperature, the curvature of the bending segment was found to be independent of the pattern length, which is highlighted by the similar trends of curvature versus temperature shown in Figure 2c, where the maximum curvature was ≈0.4 mm^{-1}.

The blocking force was measured on sample s3 by contacting the tip of the sample with the force sensor. The maximum force detected here (0.32 mN, 32 mg) was already 12 times of the actuator weight (2.7 mg) (Figure 2d).

The actuation dynamics was investigated by evaluating the time profiles of the surface temperature and corresponding curvature of sample s3 in response to a step input voltage of 20 V (Figure 2f). Such a voltage caused a temperature increase of ΔT = 80 °C, and a stable maximum temperature of 112 °C was reached in ≈10 s. The corresponding curvature profile was characterized by three different trends: rise (0–10 s, red), bent state (10–60 s, green), and recovery (60–85 s, blue). The rise time was relatively short, with the curvature rapidly increasing from the initial (off) state, which exhibited a negative curvature, as the input voltage was applied. Once the bent state (on) was reached, with a maximum curvature of nearly 0.3 mm^{-1}, it remained approximately stable as long as current was supplied. When the voltage was switched off, the actuator recovered its initial curvature within 25 s, which was the time required to reset at room temperature (see also Video S4, Supporting Information). The forward and backward curvature paths exhibited a remarkable overlap with no evidence of hysteresis (Figure 2g). To determine the operating frequency range of the actuators, we applied square wave input voltages with different frequencies to the samples. As the actuation frequency increased, we observed a reduced curvature change between the on and off states because the step voltage duration was insufficient for both the bent and relaxed states to reach stability (Figure 2e). Nevertheless, the actuator bending movement was appreciable up to 5 Hz. The long-term reliability of the actuator performance was evaluated by repetitive cycling of the actuator, up

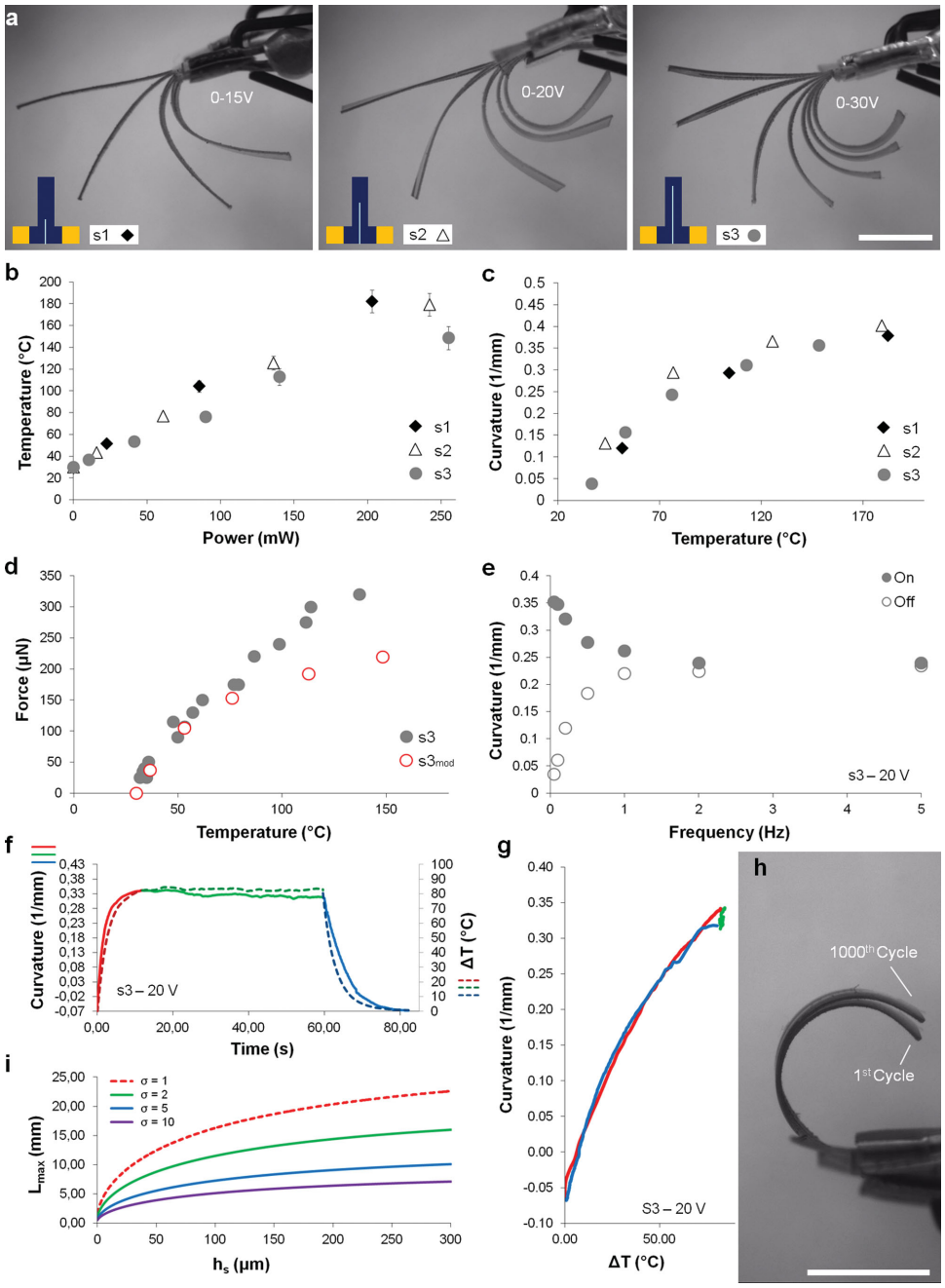

Figure 2. a) The superpositions of images taken at different input voltages for s1, s2, and s3 highlight the difference between the bending behaviors of the samples. Actuator surface temperature versus applied power. b) and curvature versus temperature c) for the three samples. d) Measured blocking force at different temperatures for sample s3 compared with the theoretical force ($s3_{mod}$). e) On/Off curvature of sample s3 powered with a square wave voltage with an amplitude of 20 V at different frequencies. Time profiles of surface temperature, curvature. f), and corresponding temperature dependence of curvature g) of sample s3 in response to a step input voltage of 20 V. h) Superposition of images taken for sample s3 before and after 1000 cycles of actuation with a square wave input voltage with a frequency of 0.05 Hz and amplitude of 20 V. All scale bars represent 5 mm. i) Actuator preliminary design chart (example): for a given thickness h_s of the PDMS layer, each curve shows the maximum actuator length L_{max} that should not be exceeded to ensure $F_b > \sigma W$, where σ is a targeted value. This chart shows that actuation is more effective for sample lengths that are less than ≈1 cm.

to 1000 cycles, and negligible changes in the curvature were observed (Figure 2h).

The static performance of the actuator was modeled using relevant expressions from linear beam theory, which was extended to a bilayer[14] (see the Supporting Information for details). In particular, we firstly obtained from the curvature (k) data the mismatch strain (α, in agreement with previous studies,[6] and we then predicted the corresponding blocking force (F_b), which is reported in Figure 2d. (labeled $s3_{mod}$) against the experimental measurements. Based on the above result, we

used the model to further characterize the application range of the actuator. In more detail, denoted by W the actuator weight, we derived the maximum length (L_{max}) beyond which the ratio F_b/W falls below a desired threshold σ, so that actuation might cease to be effective. The obtained expression reads:

$$L_{max}(h_s) = \left(\frac{E_s \alpha}{g \rho_s \sigma} h_s \xi(m,n) \right)^{1/2} \quad (1)$$

where: h_s, ρ_s, and E_s, respectively, indicate the height, the density, and Young's modulus of PDMS layer (ρ_s = 960 kg m^{-3}; E_s = 2.28 MPa, see Experimental section); g is gravity acceleration; $\xi(m,n) \equiv 3mn(1+m)/(4(1+mn))$, with $m \equiv h_f/h_s$ and $n \equiv E_f/E_s$, where h_f and E_f indicate the height and the Young's modulus of PEDOT:PSS layer (h_f = 600 nm, E_f = 1 GPa[12a]). Illustrative trends for Equation (1) are presented in Figure 2i for selected values of σ; it is clear that the developed actuator is more effective for lengths that are less than ≈1 cm, consistently with our experimental observations. For a given length, the actuator force can be enhanced by increasing the beam width. Despite its inherent simplifications, the considered model can be suitably used for the preliminary actuator design.

As previously mentioned, in addition to electrical actuation, the bilayer is able to macroscopically react to variations in environmental humidity through passive movements without requiring any electrical or thermal stimulus. The humidity-responsive passive actuation behavior of the PEDOT:PSS/PDMS films was demonstrated by placing the beam-shaped samples inside a humidity chamber and exposing them to variations in RH at a constant temperature (30 °C). The bilayer responded to the variations in humidity with a bending movement in a fully reversible manner and in the opposite direction with respect to that for electrical stimulus (**Figure 3**a). Because the humidity chamber is slow to reach a preset humidity level, it is not possible to appreciate the speed of the response from these results. The speed of the response is better evidenced, although only qualitatively, in the second part of Video S3 (Supporting Information), which shows a leaf-shaped actuator bending when a finger comes in close proximity to the PEDOT:PSS surface. A rapid response to the moisture evaporating from the skin is clear, where the leaves move away and then quickly reset back to the resting position when the finger is removed. The features of this passive behavior make this material interesting for the development of hygromorphic actuators. Because humidity is ubiquitous in real-world applications, it is important to assess how variations in RH levels influence electrically induced actuation. Indeed, different equilibrium states are established between the water content of the PEDOT:PSS film and the surrounding environmental humidity, which affects the bending radii of electrically activated actuators, with each input voltage changing with the RH level (Figure S2, Supporting Information).

The proposed bilayer actuators have applications as soft grippers, manipulators, or as active elements in millimeter-scale walking robots. Due to the mask-free and rapid fabrication process, it is easy to change the design of the actuators to meet the requirements of the target application in terms of geometry, bending behavior, and force. Site-specific electrical actuation was demonstrated with a patterned bilayer film cut in the shape of a small hand with individually addressable fingers. Five insulated and independent circuits were used to control the bending of each finger, as shown in Figure 3b (see also Video S5, Supporting Information).

As a first proof-of-concept manipulator, we created a 2 cm long, 6-finger gripper that was able to grasp and lift lightweight objects with a weight comparable with its own (Figure 3c). Moreover, a similarly shaped actuator, lying flat on a plane, was able to stand up on its legs and lift an object with a weight three times that of its own (Figure 3d). In this case, the electrical connection was established by attaching two thin copper wires to the gold electrode with silver paint.

One of the most interesting features of the proposed bilayered composites is the possibility of functioning simultaneously as a structural and functional (actuation, sensing) material. This capability indeed has long been pursued by engineers and robot designers in the search for multifunctional materials and structures for the construction of smarter and simpler tools and robots.[15] Recently, significant advances have been reported in the development of artificial muscles with tactile sensitivity (sensing muscles) which can sense by themselves while working any mechanical perturbation, not requiring additional sensors.[16]

Considering this feature, this multifunctional material can be useful for mimicking the behaviors of materials often encountered in nature. Indeed, several species of plants are capable of sensing and responding to mechanical stimuli, e.g., closing their leaves for protection (*Mimosa pudica*) or even to catch prey (*Dionaea muscipula*).[17] As an example of the potential of our approach, we attempted to imitate the behavior of *M. pudica* by exploiting the variation in electrical resistance induced in PEDOT:PSS layer structures when the bilayer is mechanically deformed. For this purpose, a simple prototype was constructed with a leaf-shaped form; this "artificial" *M. pudica* was able to close its leaves when touched (see Figure 3e and Video S5, Supporting Information). The sensing of touch is performed by dedicated electronics that monitor the resistance of the PEDOT:PSS layer with a small current through a suitable microcontroller-based system. The system triggers the Joule heating driver when a rapid resistance variation is detected. Suitable detectable variations in resistance were observed even for small deformations resulting from a gentle touch (more details on the electronics are reported in Figure S3, Supporting Information).

In conclusion, this investigation provided a straightforward and versatile method for fabricating bioinspired soft actuators and provided insight into how the relevant mechanisms of humidity sorption/desorption and Joule heating affect the actuation properties of the proposed bilayer systems. The role of geometry on the performance of the beam-shaped actuators was also addressed from experimental and theoretical perspectives. The adopted processing strategy, which consists of a few steps of spin coating, direct laser cutting, and patterning, is particularly appealing because it enables rapid and simple fabrication to test soft actuators with more complex designs. The proposed smart material structure possesses intrinsic multifunctionality, such as simultaneous structural properties, sensing, and actuation capabilities that exhibit similarities with notable examples in plants and that promote the integration of multiple functions in bioinspired soft devices/robots.

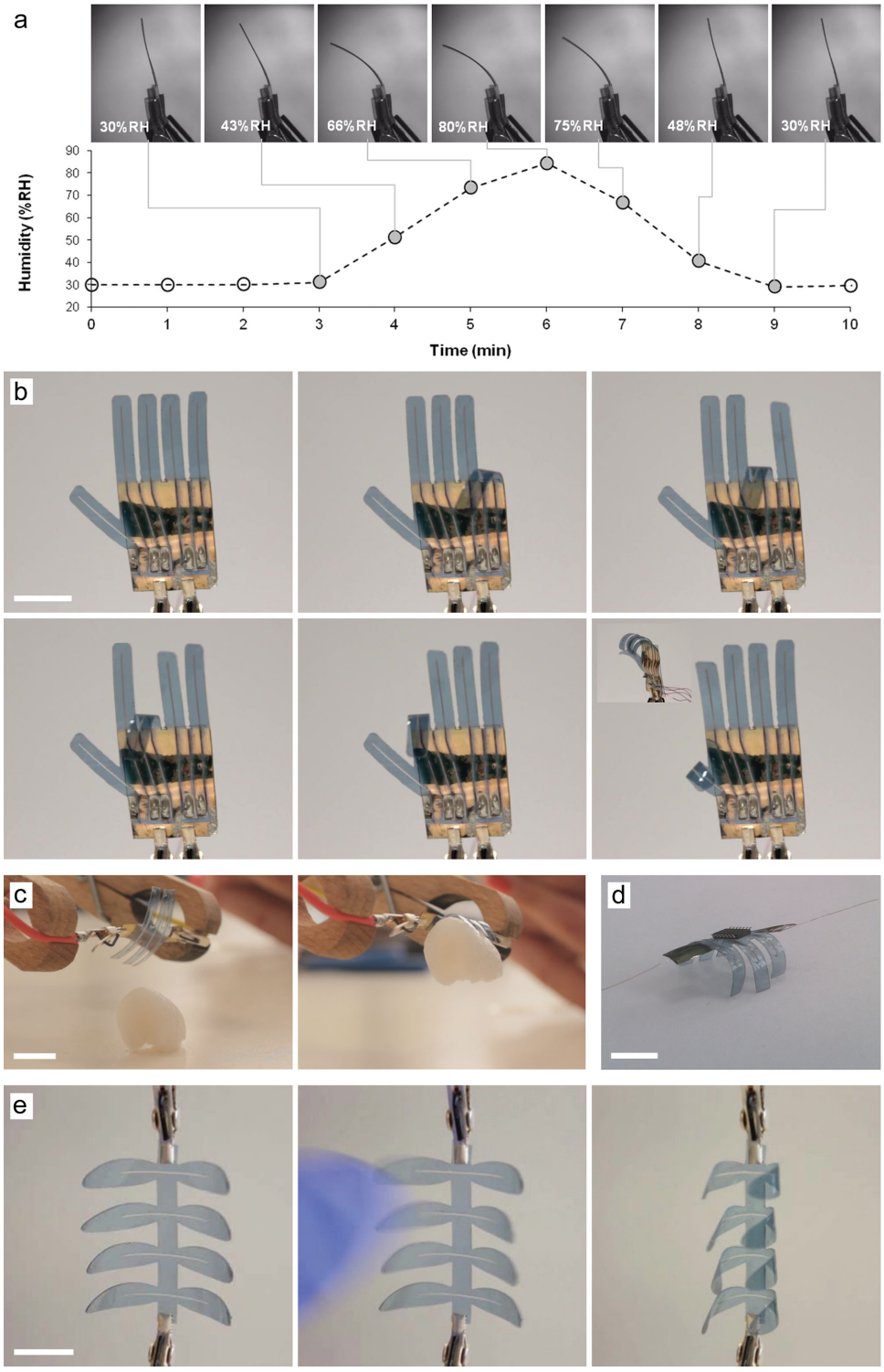

Figure 3. a) Passive bending motion of a beam caused by variations in the RH level in a humidity-controlled chamber at $T = 30$ °C (side view, PEDOT:PSS layer on the right). b) Hand-shaped actuator with individually addressable fingers. c) A 6-finger gripper prototype used to demonstrate the ability to lift a lightweight object (a piece of polystyrene foam). d) and to stand up on a plane. e) A leaf-shaped actuator (left) as a multifunctional system able to respond to touch stimuli (central) by closing its leaves (right). All scale bars represent 1 cm.

Experimental Section

Fabrication of PEDOT:PSS/PDMS Actuators: Silicon wafers (400 μm thick, p-type, boron doped, <100>, Si-Mat Silicon Materials) were silanized by placing them in a desiccator for 30 min along with a vial that contained a few drops of silanizing agent (chlorotrimethylsilane, Sigma–Aldrich). A film of PDMS (10:1 ratio of base elastomer to curing agent, Sylgard 184 silicone elastomer base and curing agent, Dow

Corning Corp.) was then spin coated onto the silanized Si substrates for 60 s at a speed of 500 rpm and then cured at $T = 95$ °C for 60 min in an oven. A subsequent air plasma treatment (Harrick PDC-002 Plasma Cleaner, Harrick Plasma) was applied with a power of $P = 5$ W for 60 s. A commercially available PEDOT:PSS aqueous dispersion (Clevios PH 1000, 1:2.5 PEDOT:PSS ratio, solid content 1.0%–1.3%; H.C. Starck Gmb) was filtered (Minisart, average pore size of 1.20 µm, Sartorius) and mixed with 1 wt% of the fluorosurfactant Zonyl-FS300 (Sigma–Aldrich). 12 layers of PEDOT:PSS were deposited by spin coating at a rate of $s = 2000$ rpm for 60 s onto the plasma-treated PDMS substrate. After each deposition step, the samples were placed on a hot plate in ambient air for 5 min at 170 °C and air plasma treated at 5 W for 10 s. Finally, the samples were subjected to a thermal treatment (1 h; $T = 170$ °C). A direct-write CO_2 laser (VersaLaser, Laser Systems) with tunable laser power, speed, and resolution was then used to cut and pattern the samples, making it feasible to fabricate a wide range of soft actuator designs and configurations. To provide the electrical input voltage to the material, gold electrodes were added to the surfaces of the actuators. A gold layer (≈100 nm thick) was deposited on the PEDOT:PSS surface by DC sputtering (Q150T S Sputter Coater, Quorum Technologies Ltd.) through dedicated shadow masks. The actuators were then peeled off from the Si substrate.

Morphology of the Actuators: Thickness measurements were performed using a P-6 stylus profilometer (KLA Tencor, USA). For the PDMS layer, measurements were performed on PDMS strips that had been peeled off from the Si substrate prior to the deposition of PEDOT:PSS. For the PEDOT:PSS layer, the PEDOT:PSS was gently scratched from the PDMS substrate with tweezers, and the height of the profile was measured across the scratch. SEM images (40° tilted view) were obtained with a Helios NanoLab 600i Dual Beam Focused ion beam/field-emission SEM instrument (FEI, USA). Images were acquired of the cross section of the bilayer cut using a razor blade.

Electrically Induced Bending: The electro-thermo-mechanical response of the actuators was investigated by recording the responses of the actuators to different step voltages with a digital optical microscope. Videos and images of the samples during the experiments were recorded with a uEye UI-2250-MM CCD camera (Imaging Development Systems, Obersulm, Germany) equipped with a Zoom 6000 zoom lens (Navitar, Rochester, NY). The temperature at the film surface was monitored by real-time thermal imaging using an IR thermal camera (A325sc, FLIR Systems, 60 Wilsonville, OR). The experiments were performed in ambient air (about 25 °C, 44% RH).

Image Processing: Curvature measurements have been performed processing images (61 px mm^{-1} resolution) of the activated samples using semiautomatic procedure implemented in Matlab (The Mathworks, Natick, MA, USA) (see Supporting Information for details).

Blocking Force Measurement: The measurement of the blocking force of the actuators was performed using silicon-based microforce sensors (FT-S540, FemtoTools). The tip of the force sensor was placed in contact with sample s3 located 8 mm from the actuator base (i.e., the clamped beam section). Once current was applied, the bending moment induced in the actuator was counteracted by the tip contact force, which was then acquired by the sensor. Samples s1 and s2 were not considered because the relatively long beam section not subjected to activation resulted in the measurement being strongly dependent on the specific location of the sensor. In other words, the conditions to properly measure the blocking moment, and thus the blocking force, were only well defined for sample s3.

PDMS Modulus Measurement: Because the model for the bending actuator is extremely sensitive to Young's modulus of the substrate and because the Young's modulus of PDMS is strongly dependent on the cross-linking process, we measured the modulus of our PDMS samples rather than using data taken from the literature. Stress/strain measurements were performed with up to a 10% applied strain on samples with dimensions of 10 mm × 3 mm × 0.12 mm using a custom dedicated set-up described elsewhere.[18]

Humidity Response: To investigate the humidity-responsive deformation of the bilayer PEDOT:PSS/PDMS actuators in a spatially homogeneous humid air environment, the samples were placed inside a climatic test chamber (CTC 256, Memmert) with controlled humidity and temperature; this chamber was equipped with a glass window to permit visual inspection of the samples. The samples were subjected to various humidity cycles at a controlled temperature (30 °C) from 30% RH up to 80% RH while simultaneously video recording the bending of the samples. The RH inside the chamber was monitored using a standard precalibrated humidity meter.

Supporting Information

Supporting Information is available from the Wiley Online Library or from the author.

Acknowledgements

The authors would like to acknowledge the contribution of the European Science Foundation COST Action MP1003 ESNAM (European Scientific Network for Artificial Muscles). This research was supported in part by PLANTOID project, FET-Open grant number: 293431, within the Seventh Framework Programme for Research of the European Commission.

Received: October 15, 2014
Revised: November 14, 2014
Published online: January 2, 2015

[1] a) S. Minko, *Responsive Polymer Materials: Design and Applications*, Wiley-Blackwell, Ames, IA, USA **2006**; b) M. A. Cohen Stuart, W. T. S. Huck, J. Genzer, M. Müller, C. Ober, M. Stamm, G. B. Sukhorukov, I. Szleifer, V. V. Tsukruk, M. Urban, F. Winnik, S. Zauscher, I. Luzinov, Sergiy Minko, *Nat. Mater.* **2010**, *9*, 101.
[2] a) E. W. H. Jager, E. Smela, O. Inganäs, *Science* **2000**, *290*, 1540; b) F. Carpi, E. Smela, *Biomedical Applications of Electroactive Polymer Actuators*, John Wiley & Sons, Chichester, UK **2009**; c) T. F. Otero, *Polym. Rev.* **2013**, *53*, 311; d) J. M. Sansiñena, V. Olazabal, T. F. Otero, C. N. Polo da Fonseca, M.-A. De Paoli, *Chem. Commun.* **1997**, *22*, 2217; e) Y. Wu, G. Alici, G. M. Spinks, G. G. Wallace, *Synth. Met.* **2006**, *156*, 1017.
[3] H. Okuzaki, T. Kuwabara, K. Funasaka, T. Saido, *Adv. Funct. Mater.* **2013**, *23*, 4400.
[4] H. Okuzaki, T. Kuwabara, T. Kunugi, *J. Polym. Sci., Part B: Polym. Phys.* **1998**, *36*, 2237.
[5] H. Okuzaki, K. Funasaka, *J. Intell. Mater. Syst. Struct.* **1999**, *10*, 465.
[6] H. Okuzaki, H. Suzukia, T. Ito, *Synth. Met.* **2009**, *159*, 2233.
[7] I. Burgert, P. Fratzl, *Philos. Trans.: Math. Phys. Eng. Sci.* **2009**, *367*, 1541.
[8] C. Dawson, J. F. V. Vincent, A.-M. Rocca, *Nature* **1997**, *290*, 668.
[9] R. Elbaum, L. Zaltzman, I. Burgert, P. Fratzl, *Science* **2007**, *316*, 884.
[10] E. Reyssat, L. Mahadevan, *J. R. Soc. Interface* **2009**, *6*, 951.
[11] A. Elschner, S. Kirchmeyer, W. Lovenich, U. Merker, K. Reuter, *PEDOT: Principles and Applications of an Intrinsically Conductive Polymer*, CRC Press, Boca Raton, FL, USA **2010**.
[12] a) F. Greco, A. Zucca, S. Taccola, A. Menciassi, T. Fujie, H. Haniuda, S. Takeoka, P. Dario, V. Mattoli, *Soft Matter* **2011**, *7*, 1064; b) S. Taccola, F. Greco, B. Mazzolai, V. Mattoli, E. W. H. Jager, *J. Micromech. Microeng.* **2013**, *23*, 117004; c) S. Taccola, F. Greco, A. Zucca, C. Innocenti, C. J. Fernández, G. Campo, C. Sangregorio,

B. Mazzolai, V. Mattoli, *ACS Appl. Mater. Interfaces* **2013**, *5*, 6324; d) F. Greco, A. Zucca, S. Taccola, B. Mazzolai, V. Mattoli, *ACS Appl. Mater. Interfaces* **2013**, *5*, 9461.

[13] a) G. Latessa, F. Brunetti, A. Reale, G. Saggio, A. Di Carlo, *Sens. Actuators B* **2009**, *139*, 304; b) S. Takamatsu, T. Takahata, M. Muraki, E. Iwase, K. Matsumoto, I. Shimoyama, *J. Micromech. Microeng.* **2010**, *20*, 075017.

[14] B. Shapiro, E. Smela, *Intell. Mater. Syst. Struct.* **2007**, *18*, 181.

[15] R. F. Gibson, *Compos. Struct.* **2010**, *92*, 2793.

[16] T. F Otero, M. T. Cortés, *Adv. Mater.* **2003**, *15*, 279; J. G. Martinez, T. F. Otero, *Sens. Actuators, B* **2014**, *195*, 365.

[17] J. Braam, *New Phytol.* **2005**, *165*, 373.

[18] F. Greco, V. Domenici, A. Desii, E. Sinibaldi, B. Zupančič, B. Zalar, B. Mazzolai, V. Mattoli, *Soft Matter* **2013**, *9*, 11405.